REPORT DOCUMENTATION PAGE

Form Approved
OMB NO. 0704-0188

1. AGENCY USE ONLY *(Leave blank)*	2. REPORT DATE	3. REPORT TYPE AND DATES COVERED
		[redacted]

4. TITLE AND SUBTITLE

[redacted]

5. FUNDING NUMBERS

DAAG55-98-1-0463

6. AUTHOR(S)

[redacted]

7. PERFORMING ORGANIZATION NAMES(S) AND ADDRESS(ES)

New Mexico State University

8. PERFORMING ORGANIZATION REPORT NUMBER

9. SPONSORING / MONITORING AGENCY NAME(S) AND ADDRESS(ES)

U.S. Army Research Office
P.O. Box 12211
Research Triangle Park, NC 27709-2211

10. SPONSORING / MONITORING AGENCY REPORT NUMBER

ARO 38696.18-EV-H

11. SUPPLEMENTARY NOTES

The views, opinions and/or findings contained in this report are those of the author(s) and should not be construed as an official Department of the Army position, policy or decision, unless so designated by other documentation.

12a. DISTRIBUTION / AVAILABILITY STATEMENT

Approved for public release; distribution unlimited.

12 b. DISTRIBUTION CODE

13. ABSTRACT *(Maximum 200 words)*

[redacted]

20010410 089

14. SUBJECT TERMS			15. NUMBER IF PAGES
			16. PRICE CODE
17. SECURITY CLASSIFICATION OR REPORT	18. SECURITY CLASSIFICATION OF THIS PAGE	19. SECURITY CLASSIFICATION OF ABSTRACT	20. LIMITATION OF ABSTRACT
UNCLASSIFIED	UNCLASSIFIED	UNCLASSIFIED	UL

A REEXAMINATION OF ACOUSTIC SCATTERING IN THE ATMOSPHERE USING AN IMPROVED MODEL FOR THE TURBULENCE SPECTRUM

D. Keith Wilson*
U.S. Army Research Laboratory
2800 Powder Mill Rd, Adelphi, MD 20783
Phone: 301-394-2099; FAX: 301-394-1155
email: dkwilson@arl.mil

Vladimir E. Ostashev
NOAA/ETL Environmental Technologies Laboratory
325 Broadway, Boulder, CO 80303
email: vostashev@etl.noaa.gov

ABSTRACT

Sound waves propagating near the ground are scattered by random fluctuations in the velocity and temperature fields. We revisit the problem of scattering of sound by turbulence using an improved von Kármán-type model for the atmospheric turbulence spectrum. The new model incorporates large boundary-layer scale eddies generated by atmospheric convection, as well as smaller height-scale eddies generated by surface-layer shear. We show that velocity fluctuations from the large convective eddies are typically the cause of random signal behavior for low acoustical frequencies and line-of-sight propagation. For higher frequencies and scattering angles, the shear turbulence becomes more important, with the relative importance of scattering by temperature and velocity fluctuations depending on the degree of atmospheric convection. By applying the new model to monostatic sodar systems, we find that sodar measurements of the temperature structure parameter can be systematically contaminated by the velocity structure parameter in strong wind conditions. We also discuss how the new model can be used to determine appropriate baselines for direction-finding arrays when there is significant degradation of signal coherence caused by turbulence.

INTRODUCTION

Turbulence plays an important role in the propagation of sound waves through the atmosphere: it causes random fluctuations in the amplitude and phase of acoustic signals, diminishes wavefront coherence, and randomly scatters energy into shadow regions (regions where direct sound transmission is blocked by refraction or hard objects). As a result, modeling of the spectrum of atmospheric turbulence has become an important issue in acoustics. Of primary interest are the wind and temperature spectra, since these fields have the strongest effect on sound waves.

Turbulent motions in the atmosphere span a broad range of spatial scales, from less than a millimeter to a kilometer. The spectrum of these motions can be partitioned into three distinct

spectral regions or *subranges*. In order of decreasing eddy size, these are the *energy-containing* (or *source*), the *inertial*, and the *dissipation* subranges (Hinze, 1975). Much previous research on wave scattering by turbulence has focused on the contribution coming from the relatively small eddies of the inertial and dissipation subranges. Kolmogorov (1941) developed a simple statistical scaling for characterizing the inertial-subrange part of the spectrum, and Tatarskii (1971) and others succeeded in applying Kolmogorov's spectrum to wave scattering.

The dissipation subrange can generally be ignored for outdoor sound propagation. For most frequencies within the audible range, dissipation-subrange eddies are too small (less than about 1 cm) to affect the propagation. Therefore the energy-containing and inertial subranges play the primary role. Broadly speaking, the large-scale (100 m and larger) eddies of the energy-containing subrange drive acoustic phase fluctuations, whereas smaller-scale motions with sizes on the order of an acoustic wavelength (10 cm to 10 m) drive the amplitude fluctuations. However, the interplay between the propagation geometry, refraction, scattering, and acoustic wavelength often complicates this idealized picture.

The need for a practical spectral model valid in both the energy-containing and inertial subranges has forced the atmospheric acoustics research community to look beyond Kolmogorov's model. Wave propagation calculations furthermore require a three-dimensional spectrum for the turbulence: the structure in the direction of propagation, as well as the transverse directions, must be known. Hence the one-dimensional models developed by micrometeorologists from time series (such as Kaimal et al (1972) and Højstrup (1982)) cannot be used directly.

For these reasons many papers on sound scattering in the atmosphere have used Gaussian spectral models instead of Kolmogorov's (e.g., Daigle et al, 1983; Daigle et al., 1986; Johnson et al, 1987; Wilson and Thomson, 1994). The Gaussian model is simple and reasonable for the energy-containing subrange. Unfortunately, it is very poor for the inertial subrange. To improve on the behavior of the Gaussian models, von Kármán-type models have recently been considered (Ostashev, 1997; Ostashev et al, 1998; Wilson 1998). These models behave similarly to Gaussian ones in the energy-containing subrange, yet still reproduce Kolmogorov's spectrum in the intertial subrange.

This paper describes our recently developed, isotropic von Kármán model for the atmospheric wind and temperature spectra. As described in the following section, the model parameters are determined from atmospheric turbulence similarity scaling theories and previous atmospheric measurements. After introducing the model, we discuss its reduction for the two special cases where eddies in either the energy-containing or inertial subrange dominate the scattering. Lastly, we consider predictions from the model for two important applications: monostatic sodar systems and ground-based acoustic arrays used for direction finding.

THE VON KÁRMÁN TURBULENCE MODEL

The von Kármán model for the turbulent velocity fluctuations is based on the following spectrum for the specific turbulent kinetic energy (Ostashev, 1997; Ostashev et al, 1998; Wilson 1998):

$$E_v\left(\kappa;\sigma_v^2,\ell_v\right)=\frac{4\Gamma(17/6)}{\sqrt{\pi}\Gamma(1/3)}\frac{\sigma_v^2\kappa^4\ell_v^5}{\left(1+\kappa^2\ell_v^2\right)^{17/6}}, \tag{1}$$

where κ is the turbulence wavenumber, σ_v^2 the variance of one of the velocity components, and ℓ_v a length scale representative of the transition between the energy-containing and inertial subranges. (Note that $E(\kappa)$ in this paper is equivalent to $4\pi\kappa^2 F(\kappa)$, and ℓ equivalent to K_0^{-1}, in Ostashev (1997) and Ostashev et al (1998).) The spectral density $\Phi_{ij}(\ )$ between the i and j components of the velocity field follows from the energy spectrum (Batchelor, 1953):

$$\Phi_{ij}(\ ) = \frac{E(\kappa)}{4\pi\kappa^4}\left(\kappa^2\delta_{ij} - \kappa_i\kappa_j\right). \tag{2}$$

The integral of one of the autospectra (the spectra for which $i = j$) over the three-dimensional wavenumber space equals the variance σ_v^2.

For a scalar quantity such as the temperature field, the spectral density is modeled by the equation

$$\Phi_T(\kappa;\sigma_T^2,\ell_T) = \frac{\Gamma(11/6)}{\pi^{3/2}\Gamma(1/3)}\frac{\sigma_T^2\ell_T^3}{\left(1+\kappa^2\ell_T^2\right)^{11/6}}. \tag{3}$$

(Equation (3) is equivalent to (6.44) in Ostashev (1997), as can be shown by substituting for C_T^2 with (6.49), applying several identities for gamma functions, and replacing K_0 by ℓ_T.)

Given equations (1) to (3) for the spectral densities of the velocity and temperature fields, our next step is to determine appropriate values for the variance and length-scale parameters. In boundary-layer meteorology, parameters such as these are usually estimated through the use of turbulence similarity scaling theories. In the following we consider separate scalings for shear- and buoyancy-produced turbulence, and then combine the scalings.

Shear-produced turbulence. When near-ground turbulence is produced predominantly by wind shear, the parameters generally accepted as being most important are the friction velocity, u_*; the height from the ground, z; and the kinematic surface heat flux, Q_s. A temperature scale T_* is formed by dividing Q_s by u_*. The velocity variance should therefore be proportional to u_*^2, the temperature variance to T_*^2, and the length scales to z. Based on comparisons with existing atmospheric data and spectral models, Wilson (2000) determined $\sigma_v^2 = 3.0u_*^2$ and $\ell_v = 1.8z$ for the velocity field. Stull (1988) suggests $\sigma_T^2 = 4.0T_*^2$ based on previous results in the literature, and Ostashev and Wilson (2000) found $\ell_T = 1.5z[\Gamma(1/3)/\sqrt{\pi}\Gamma(5/6)] = 2.0z$.

Buoyancy-produced turbulence. Atmospheric data show that the horizontal velocity components and the temperature obey different similarity scaling rules when buoyancy production of turbulence (primarily heating of the layer of air adjacent to the ground) is strong. For both fields, the kinematic surface heat flux Q_s and the Boussinesq buoyancy parameter $\beta = g/T_s$ (where g is gravitational acceleration and T_s surface temperature) appear important. However, the appropriate length scale for the horizontal velocity fluctuations is the boundary-layer inversion height, z_i, whereas for temperature it is the height from the ground, z. The velocity scale formed from Q_s, β, and z_i is $w_* = (Q_s\beta z_i)^{1/3}$. The temperature scale formed

from Q_s, β, and z is $\theta_f = Q_s / u_f$, where $u_f = (Q_s \beta z)^{1/3}$. Wilson (2000) determined $\sigma_v^2 = 0.35 w_*^2$ and $\ell_v = 0.23 z_i$ for the velocity field, while Stull (1988) suggests $\sigma_T^2 = 1.9\theta_*^2$, and Ostashev and Wilson (2000) $\ell_T = 1.4z$, for the temperature field.

Shear-buoyancy combination. For the velocity field, the combined effects of shear and buoyancy production are often dealt with simply by adding together spectra representing the shear and buoyancy modes of production (Højstrup, 1982; Peltier et al, 1996). Therefore the overall energy spectrum would be

$$E(\kappa) = E_v(\kappa; 3.0u_*^2, 1.5z) + E_v(\kappa; 0.35w_*^2, 0.23z_i), \tag{4}$$

where E_v is given by equation (1). Methods for combining the shear and buoyancy contributions to the temperature spectrum are not as well established. Peltier et al (1996) suggested combining the two contributions in reciprocal (parallel) fashion. A drawback of this approach is that we can no longer analytically integrate the combined spectrum. Given that the length scales for shear and buoyancy turbulence are very close, however, it is not critically important how the spectra are combined: we could use equation (3) directly for the overall spectrum, so long as the *variance* is modeled well. The following equation for the temperature interpolates smoothly between the shear- and buoyancy-production limits (Wilson and Thomson, 1994):

$$\sigma_T^2 = 4.0T_*^2 [1 + 10(-z / L_{mo})]^{-2/3}, \tag{5}$$

where $L_{mo} = -u_*^3 / k_v \beta Q_s$ is called the *Monin-Obukhov length* ($k_v \approx 0.4$ is von Kármán's constant). The following equation (based on a derivation in Ostashev and Wilson (2000)) for the temperature length scale interpolates in similar fashion:

$$\ell_T = 2.0z \frac{1 + 7.0(-z / L_{mo})}{1 + 10(-z / L_{mo})}. \tag{6}$$

Given equations (1) to (6), other quantities of interest relevant to scattering (such as integrated spectra, correlation functions, and structure-function parameters) can be determined by performing various integrations and transformations. The procedures are summarized by Tatarskii (1971) and Ostashev (1997). In the remainder of this paper we consider various applications of these equations to acoustic scattering in the near-ground atmosphere. Comparisons are also made between the relative strengths of scattering by wind velocity and temperature fluctuations.

SCATTERING IN THE ENERGY-CONTAINING SUBRANGE

It was mentioned in the Introduction that for many situations acoustic scattering in the atmosphere is affected mainly by large-scale turbulence in the energy-containing subrange. For example, if $x/(kL_T^2) >> 1$ and $x/(kL_v^2) >> 1$, the variances of the log-amplitude and phase fluctuations (for both planar and spherical waves) are nearly the same and given by (Flatté et al, 1979; Ostashev and Wilson, 2000)

$$\langle \chi^2 \rangle = \langle \phi^2 \rangle = \frac{k^2 x}{4}\left(L_T \frac{\sigma_T^2}{T_0^2} + L_\upsilon \frac{4\sigma_\upsilon^2}{c_0^2} \right). \tag{7}$$

Here x is the horizontal propagation distance, $k = 2\pi f / c_0$ is the acoustic wavenumber, χ is the log-amplitude fluctuation, ϕ is the phase fluctuation, the L's are integral length scales, f is the frequency, and T_0 and c_0 are representative values of the temperature and sound speed. It follows that the ratio N of the velocity and temperature contributions to the moments in the energy-containing subrange is given by

$$N = \frac{4L_\upsilon \sigma_\upsilon^2 / c_0^2}{L_T \sigma_T^2 / T_0^2}. \tag{8}$$

The model in the previous section implies that the variance for the velocity field is simply the sum of the contributions from shear and buoyancy turbulence, i.e., $\sigma_\upsilon^2 = 3.0u_*^2 + 0.35w_*^2$. The velocity field integral length scale corresponding to the model is (Wilson, 2000)

$$L_\upsilon = 1.3z \frac{1 + 0.022(z_i / z)(-z_i / L_{mo})^{2/3}}{1 + 0.22(-z_i / L_{mo})^{2/3}}. \tag{9}$$

An equation for the temperature variance was given earlier (equation (5)). The integral length scale for temperature, L_T, is equal to $[\sqrt{\pi}\Gamma(5/6)/\Gamma(1/3)]\ell_T$, with ℓ_T given by equation (6).

The height dependence of the log-amplitude variance for scattering in the energy-containing subrange is shown in Figure 1. We see that scattering is stronger in sunny conditions than in cloudy ones, and is nearly independent of height near the ground. In this region, velocity fluctuations from the buoyantly produced z_i-scale eddies are the main contributor to scattering. In very windy conditions, for heights larger than 10 m, shear-produced velocity fluctuations take over as the main contributor to scattering.

The ratio of velocity and temperature contributions (equation 8) is shown in Figure 2. For scattering in the energy-containing subrange, the velocity fluctuations are always much more important than the temperature fluctuations, even for sunny, light wind conditions. This is particularly so near the ground.

SCATTERING IN THE INTERTIAL SUBRANGE

The inertial subrange consists of wavenumbers such that $\kappa\ell >> 1$. In this limit the energy spectrum of the velocity fluctuations is

$$E(\kappa) = \frac{4\Gamma(17/6)}{\sqrt{\pi}\Gamma(1/3)} \sigma_\upsilon^2 \kappa^{-5/3} \ell_\upsilon^{-2/3} = \frac{55}{27\Gamma(1/3)} C_\upsilon^2 \kappa^{-5/3}. \tag{10}$$

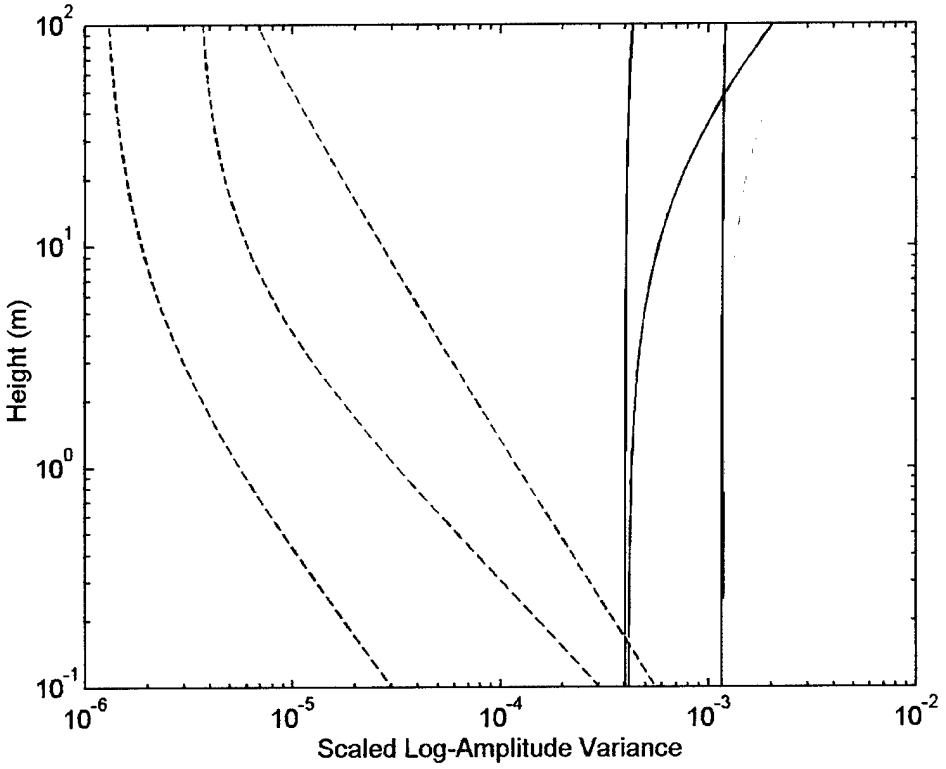

Figure 1. Height dependence of the scaled log-amplitude variance. Solid lines are for scattering in the energy-containing subrange (plotted is $L_T\sigma_T^2/4T_0^2 + L_\upsilon\sigma_\upsilon^2/c_0^2$, with the L's in meters), and dashed lines are for the inertial subrange (plotted is $C_T^2/T_0^2 + 22C_\upsilon^2/3c_0^2$). Blue: cloudy with light wind ($u_* = 0.1$ m/s, $T_* = -0.33$ K); green: cloudy with strong wind ($u_* = 0.7$ m/s, $T_* = -0.046$ K); red: sunny with light wind ($u_* = 0.1$ m/s, $T_* = -1.6$ K); yellow: sunny with strong wind ($u_* = 0.7$ m/s, $T_* = -0.23$ K). For all cases, $z_i = 1000$ m.

For the spectral density of temperature,

$$\Phi_T(\ ) = \frac{\Gamma(11/6)}{\pi^{3/2}\Gamma(1/3)}\sigma_T^2\kappa^{-11/3}\ell_T^{-2/3} = \frac{5}{18\pi\Gamma(1/3)}C_T^2\kappa^{-11/3}. \tag{11}$$

The equalities involving the variance in length scale in equations (10) and (11) are the large-wavenumber limits of equations (1) and (3); the second pair of equalities, involving the structure-function parameters C_υ^2 and C_T^2, follow from equation (6.38) in Ostashev (1997). Equations (10) and (11) imply that

$$C_\upsilon^2 = \frac{3\Gamma(5/6)}{\sqrt{\pi}}\sigma_\upsilon^2\ell_\upsilon^{-2/3}, \text{ and } C_T^2 = \frac{3\Gamma(5/6)}{\sqrt{\pi}}\sigma_T^2\ell_T^{-2/3}. \tag{12}$$

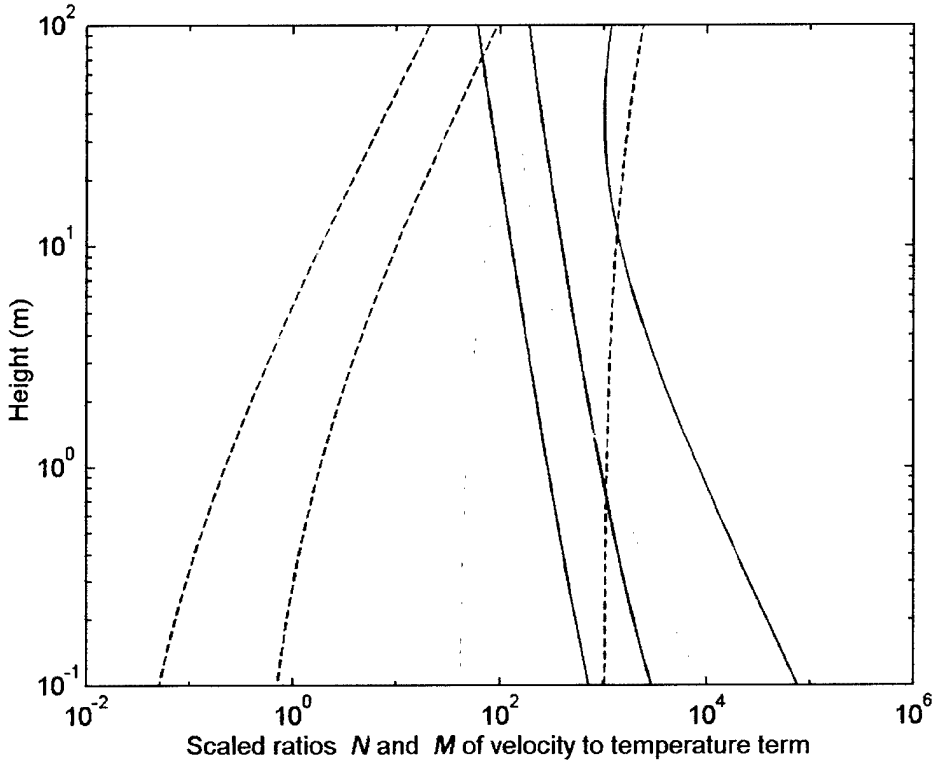

Figure 2. Height dependence of the scaled ratios M and N of the velocity term to the temperature term for scattering of sound. Legend is the same as Figure 1.

Equation (4) implies that the contributions to C_υ^2 from shear and buoyancy turbulence simply sum together. The result is the equation

$$C_\upsilon^2 = 3.9\frac{u_*^2}{z^{2/3}}\left[1+0.85(-z/L_{mo})^{2/3}\right]. \tag{13}$$

When equations (5) and (6) are used to calculate C_T^2, a relationship for C_T^2 originally suggested by Wyngaard et al (1971) results:

$$C_T^2 = 4.9\frac{T_*^2}{z^{2/3}}\left[1+7.0(-z/L_{mo})\right]^{-2/3}. \tag{14}$$

It is shown in section 7.3.1 of Ostashev (1997) that all statistical moments of a sound field scattered by inertial-subrange turbulence are proportional to $C_T^2/T_0^2 + 22C_\upsilon^2/3c_0^2$. For example, the variance of log-amplitude fluctuations of a plane sound wave is given by

$$\left\langle \chi^2 \right\rangle = 0.077 k^{7/6} x^{11/6} \left(\frac{C_T^2}{T_0^2} + \frac{22}{3} \frac{C_v^2}{c_0^2} \right). \tag{15}$$

The ratio M of the velocity and temperature contributions for inertial-subrange scattering is therefore

$$M = \frac{22}{3} \frac{C_v^2 / c_0^2}{C_T^2 / T_0^2}. \tag{16}$$

The height dependence of the log-amplitude variance for scattering in the inertial subrange is shown in Figure 1. The ratio of velocity and temperature contributions (equation 16) is shown in Figure 2. In contrast to energy-containing-subrange scattering, inertial-subrange scattering decreases rapidly with increasing height. Its strength is determined mainly by the degree of windiness, rather than the heat flux. The contribution from velocity fluctuations is normally stronger than that from temperature fluctuations, although near the ground in light wind conditions the temperature contribution can be larger.

MONOSTATIC SODAR SYSTEMS

In a paper soon to be published (Ostashev and Wilson, 2000), we consider the implications of the preceding turbulence model for measurements made with monostatic sodar systems. When sodars are operated with a vertical beam, it is normally assumed that the scattering results solely from temperature fluctuations (C_T^2). However, due to the height-dependence of the mean horizontal wind speed, turbulent velocity fluctuations (C_V^2) can significantly contaminate the sodar measurements in strong winds. Figure 3 is a plot, for a vertically directed beam, of the ratio $\hat{\sigma}_m$ of the actual scattering cross section to that given by Monin's (1962) classical equation versus the ratio M for different values of the wind velocity at the height of the scattering volume. Monin's equation predicts that the scattering cross section depends solely on C_T^2 for pure backscattering. Values of the ratio $\hat{\sigma}_m$ larger than 1 in Figure 3 imply contamination by C_V^2. For wind speeds at the scattering height greater than about 10 m/s, and values of the ratio M greater than about 1000, there is indeed significantly more scattering than predicted by Monin's equation. The calculations in this figure are somewhat idealized in that the mean vertical profiles for sound speed and wind speed are assumed to be linear.

We have also performed numerical calculations for mean vertical profiles that obey Monin-Obukhov similarity. For a scattering height of $0.5 z_i$ (with $z_i = 1000$ m), we obtained the following results:

- Sunny and light wind ($u_* = 0.1$ m/s, $T_* = -1.6$ K): $M = 554$, $\hat{\sigma}_m$=1.01.
- Sunny and moderate wind ($u_* = 0.3$ m/s, $T_* = -0.54$ K): $M = 572$, $\hat{\sigma}_m$=1.12.
- Sunny and strong wind ($u_* = 0.7$ m/s, $T_* = -0.23$ K): $M = 874$, $\hat{\sigma}_m$=2.55.
- Cloudy and light wind ($u_* = 0.1$ m/s, $T_* = -0.33$ K): $M = 1520$, $\hat{\sigma}_m$=1.02.

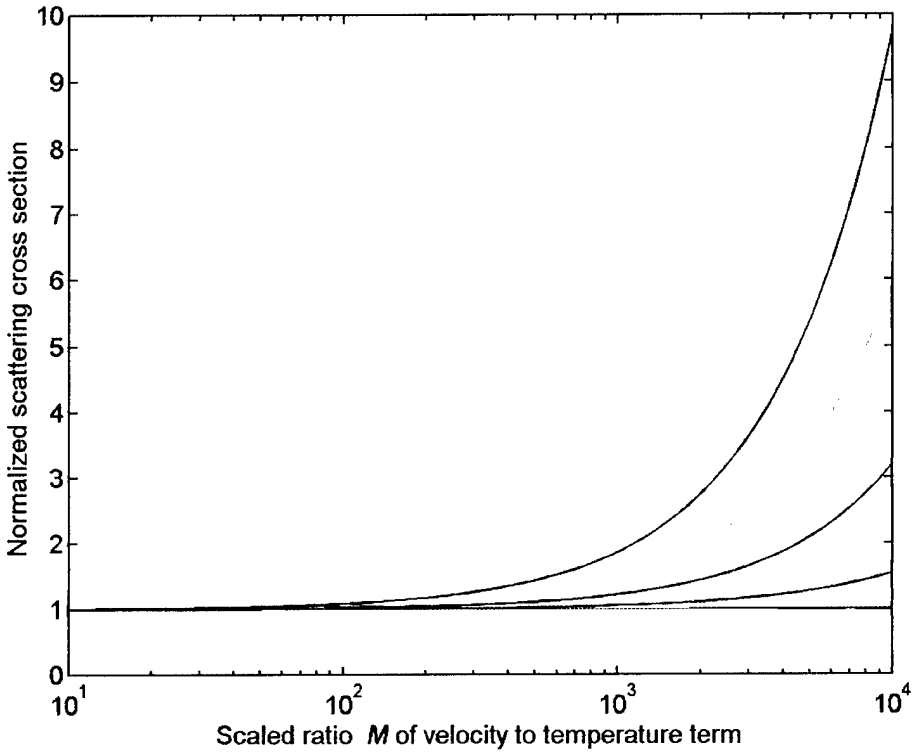

Figure 3. Normalized backscattering cross section $\hat{\sigma}_m(180°)$ for a monostatic sodar versus the ratio $M = (22/3)(C_v^2/c_0^2)/(C_T^2/T_0^2)$ for different values of the horizontal wind velocity at the height of the scattering volume. The lines correspond to 0 m/s (blue), 5 m/s (green), 10 m/s (red), 15 m/s (yellow), and 20 m/s (purple).

- Cloudy and moderate wind ($u_* = 0.3$ m/s, $T_* = -0.11$ K): $M = 1970$, $\hat{\sigma}_m$=1.56.
- Cloudy and strong wind ($u_* = 0.7$ m/s, $T_* = -0.046$ K): $M = 4760$, $\hat{\sigma}_m$=11.33.

In sunny weather with strong wind, or in cloudy weather with moderate to strong wind, the scattering cross section is significantly affected by atmospheric winds and velocity fluctuations.

COHERENCE AND DIRECTION-FINDING ARRAYS

Most new U.S. Army acoustical systems use small, ground-based beamforming arrays (footprint smaller than about one square meter) to determine the horizontal bearing angle of sound-emitting targets. The ability of these arrays to track targets is limited by the coherence between the signals received by the array sensors. Propagation through turbulence reduces the coherence, as illustrated in Figure 4.

When the integral length scale of the refractive index field is *large* compared to the separation between the sensors, the wavefronts (viewed on the array scale) have a smooth,

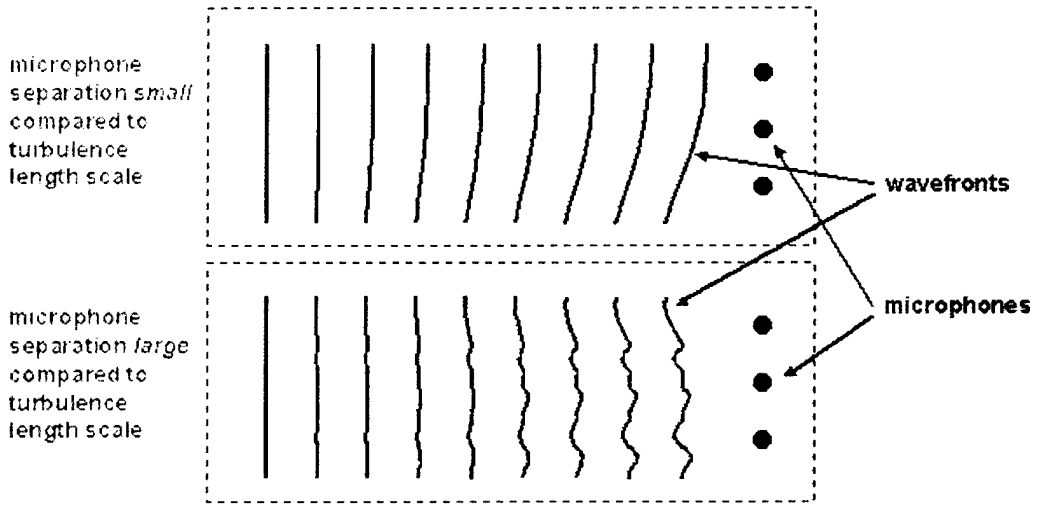

Figure 4. Illustration of random variations in propagating wavefronts resulting from propagation through turbulence.

nearly planar appearance when they arrive at the array (upper Figure 4). (On a scale much smaller than the microphone separation the wavefronts may have a rough, random appearance.) For the opposite extreme, when the sensor separations are large compared to the integral length scale (lower Figure 4), the wavefronts take on a rough, random appearance. In analogy to optics, the former situation would correspond to variations in the apparent position of an image. The latter situation would correspond to random distortions in the image.

Note that both situations manifest themselves as a reduction in coherence (consistent amplitude and phase relationship) between the sensor signals. Having a sensor separation that is small compared to the integral length scale does *not* guarantee that the coherence is good *on average* since the phase fluctuations can still be large. The variations in angle of arrival would still randomize the phase relationship between the received signals. One important practical distinction between the two situations is that if the sensor separation is large compared to the integral length scale, there is no *additional* loss in coherence from moving sensors farther apart. The mutual phase variations between the sensors are already fully saturated. For relatively small separations, however, increasing the sensor separation increases the random phase differentials. Therefore it is important that one know the characteristic integral length scale for the sound field when designing an array.

Based on equation (20) to follow, the effective integral length scale for the acoustic index-of-refraction fluctuations (parallel to the propagation direction) is

$$L_{eff} = \frac{\sigma_T^2 L_T / T_0^2 + 4\sigma_\upsilon^2 L_\upsilon / c_0^2}{\sigma_T^2 / T_0^2 + 4\sigma_\upsilon^2 / c_0^2}. \tag{17}$$

Figure 5 shows calculations of L_{eff} from our model. The longest values for the integral length scale (>100 m) occur when the wind is weak there is little heat flux from the ground to the air (cloudy conditions). In these situations shear-induced velocity fluctuations and temperature

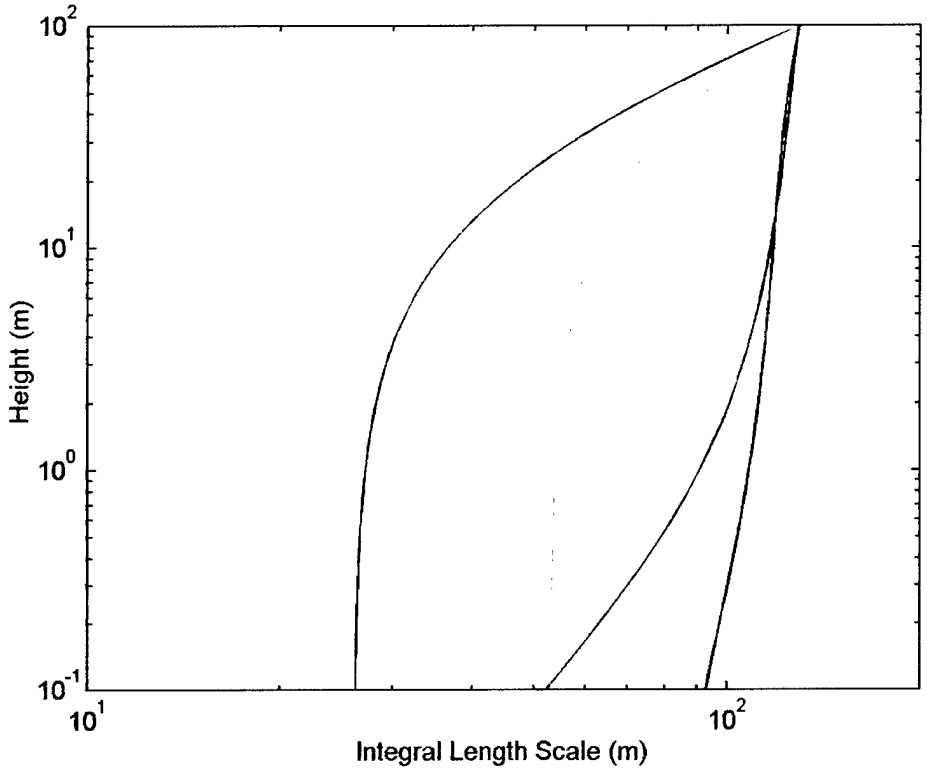

Figure 5. Effective integral length scale for several atmospheric conditions. Legend is the same as Figure 1.

fluctuations have little effect on the length scale. The shortest values (<20 m) occur near the ground when the wind and heat flux are both strong.

Based on the parabolic and Markov approximations, the coherence for a propagating wave can be written in the general form

$$\Gamma(f,x,r) = \exp[-\alpha(f,r)x], \tag{18}$$

where r is the separation between the sensors perpendicular to the propagation path, and f the frequency of the sound wave. The quantity $\alpha(f,r)$ can be thought of as an attenuation coefficient for the coherence. As shown by Ostashev (1997) for spherical wave propagation through a random medium with both temperature and velocity fluctuations, the value of $\alpha(f,r)$ is

$$\alpha(f,r) = \pi^2 k^2 \int_0^1 \int_0^\infty [1 - J_0(\kappa_\perp rt)]\, \Phi_{eff}(0,\kappa_\perp)\, d\kappa_\perp\, dt. \tag{19}$$

Here J_0 is the Bessel function of the first kind, and the wavenumber vector has been decomposed as $\quad = {}_1 + {}_\perp$, where ${}_\perp$ is the component perpendicular to the direction of propagation. The effective spectrum for the acoustic index-of-refraction fluctuations is given by

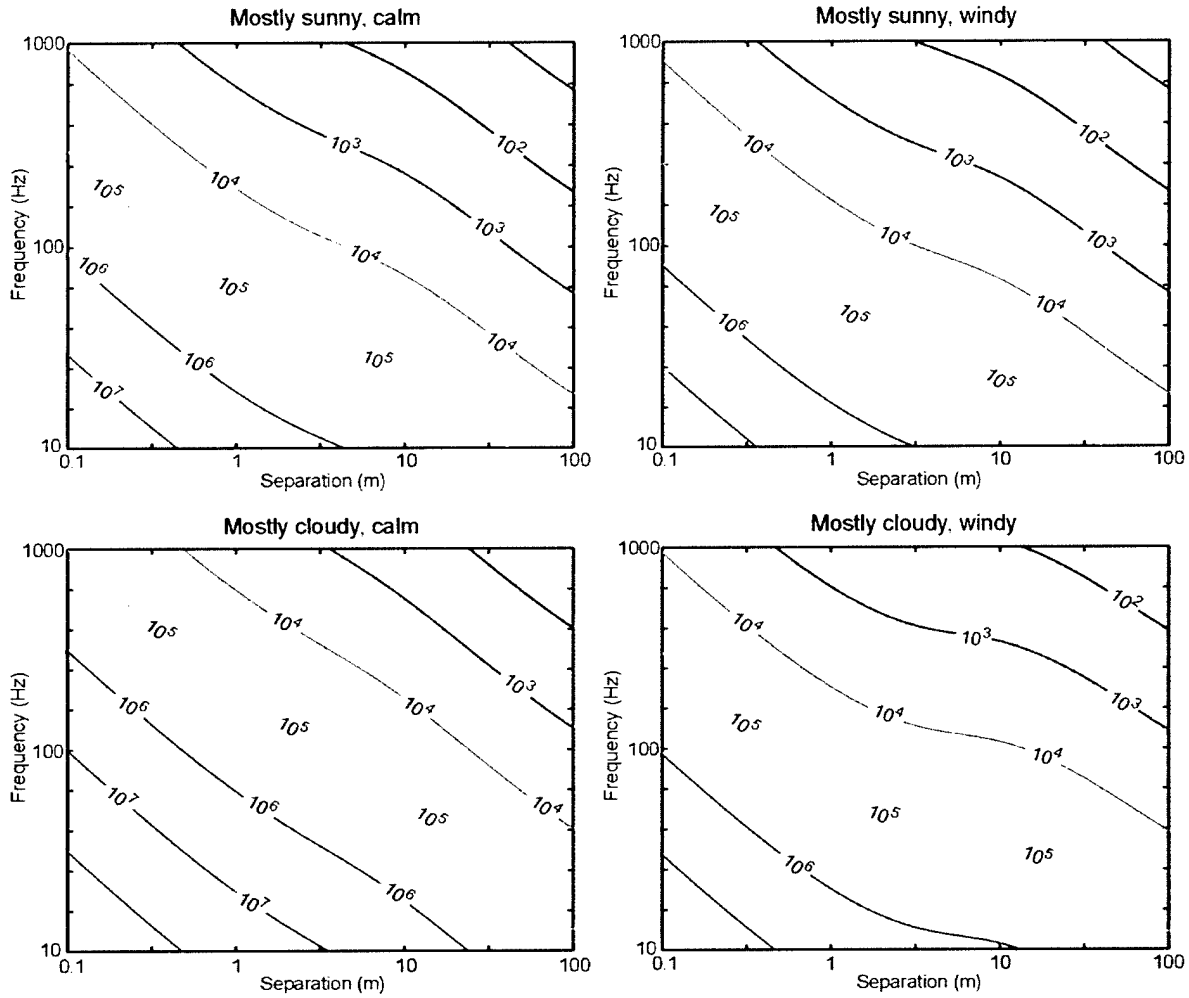

Figure 6. Inverse attenuation coefficient for the coherence (i.e., the distance at which the signal coherence diminishes to $1/e$) for four example atmospheric states. The contours are in units of meters, as a function of the acoustic frequency and the separation between the sensors. Upper left: mostly sunny and calm conditions ($u_* = 0.1$ m/s and $T_* = -3.3$ K). Upper right: mostly sunny and windy conditions ($u_* = 0.5$ m/s, $T_* = -0.65$ K). Lower left: mostly cloudy and calm conditions ($u_* = 0.1$ m/s, $T_* = -0.33$ K). Lower right: mostly cloudy and windy conditions ($u_* = 0.5$ m/s, $T_* = -0.065$ K). For all cases, $z_i = 1000$ m.

$$\Phi_{eff}(\ _1,\ _\perp) = \frac{\Phi_T(\ )}{T_0^2} + \frac{4\Phi_{11}(\ )}{c_0^2}. \tag{20}$$

Note that it is primarily the wind fluctuations in the direction of wave propagation that affect the coherence.

Calculations of $\alpha^{-1}(f,r)$ for the four different atmospheric conditions are shown in Figure 6. The contours represent the distance at which the signal becomes incoherent, as a function of frequency and sensor separation. We see that sunny and windy conditions constitute the least favorable propagation condition. Large, vigorous turbulent eddies forming in such conditions weaken acoustic signal coherence considerably. The most favorable propagation condition is mostly cloudy and calm, since only very weak turbulence is present in this case. The model calculations show, for a sensor separation of 1 m and frequency of 1000 Hz, that coherent propagation generally occurs only out to distances of several hundred meters. Fortunately the situation improves dramatically for lower frequencies; for 1-m separations at 100 Hz, coherent propagation persists to well over 10 km. If the separation is increased to 10 m, one can still expect good coherence for propagation distances of several kilometers.

Some caveats must be kept in mind regarding these calculations. First, little experimental data on acoustic coherence degradation by atmospheric turbulence has been collected and analyzed. This situation is quite surprising, and demands rectification, given the importance of the phenomenon for modern acoustic direction-finding systems. Second, the calculations are for "line-of-sight" (straight line) propagation. Reflections from the ground and refraction from atmospheric wind and temperature gradients (with subsequent creation of refractive shadow regions) both affect the coherence. Research into these effects is still at an early stage (Daigle et al, 1986; Havelock et al, 1995; Ostashev and Goedecke, 1998).

CONCLUSIONS AND RECOMMENDATIONS

The turbulence model in this paper was systematically developed from similarity theory and previous, well-accepted experimental results for the atmospheric boundary layer. Because it is based on von Kármán's three-dimensional turbulence spectrum, it can be readily applied to acoustic wave propagation problems. It is a valuable improvement over previous models based on the Kolmogorov or Gaussian spectra, in that it provides reasonable results across the entire range of sizes of boundary-layer eddies. It should work well for atmospheric conditions ranging from neutral to highly unstable.

The model in this paper is, however, imperfect in that it does not account for some known features of atmospheric turbulence such as anisotropy. For example, shear forces are known to stretch eddies in the direction of the mean wind. For this reason we have recently begun applying Mann's (1994) spectral model for a shear surface layer to acoustical calculations.

Another aspect of atmospheric turbulence not accounted for by the model is the "gustiness" of the wind. Large boundary-layer scale eddies cause the wind to gust on time scales lasting several minutes. These gusts can create locally high wind shear. Hence the present model is misleading in predicting the absence of shear-generated turbulence at very low *mean* wind speeds. It is also probable that the strength of the large-scale eddies diminishes somewhat near the ground, whereas the present model predicts a height-independent variance from these eddies.

Besides turbulence, other random atmospheric behavior can affect sound waves. In particular, during stable nighttime conditions, turbulence is suppressed and gravity waves probably play the primary role in randomizing acoustic propagation. This phenomenon has gone nearly unstudied in acoustics, and needs to be addressed, since acoustical systems offer particular tactical advantages during the nighttime.

ACKNOWLEDGMENTS

V. Ostashev's research was supported by an NRC-ETL Research Associateship and by the U.S. Army Research Office under contract number DAAG55-98-1-0463 (administered by W. Bach).

REFERENCES

Batchelor, G. K. (1953): *The Theory of Homogeneous Turbulence.* Cambridge U.P., Cambridge, U.K.

Daigle, G. A., T. F. W. Embleton, and J. E. Piercy (1986): Propagation of sound in the presence of gradients and turbulence near the ground. *J. Acoust. Soc. Am.* **79**, 613–627.

Daigle, G. A., J. E. Piercy, and T. F. W. Embleton (1983): Line-of-sight propagation through atmospheric turbulence near the ground. *J. Acoust. Soc. Am.* **74**, 1505–1513.

Flatté, S. M., R. Dashen, W. H. Munk, K. M. Watson, and F. Zachariasen (1979): *Sound Transmission through a Fluctuating Ocean.* Cambridge U. P., New York.

Havelock, D. I., X. Di, G. A. Daigle, and M. R. Stinson (1995): Spatial coherence of a sound field in a refractive shadow: Comparison of simulation and experiment. *J. Acoust. Soc. Am.* **98**, 2289–2302.

Hinze, J. O. (1975): *Turbulence.* McGraw-Hill, New York.

Højstrup, J. (1982): Velocity spectra in the unstable planetary boundary layer. *J. Atmos. Sci.* **39**, 2239–2248.

Johnson, M. A., R. Raspet, and M. T. Boback (1987): A turbulence model for sound propagation from an elevated source above ground level. *J. Acoust. Soc. Am.* **81**, 638–646.

Kaimal, J. C., J. C. Wyngaard, Y. Izumi, and O. R. Coté (1972): Spectral characteristics of surface layer turbulence. *Q. J. R. Meteorol. Soc.* **98**, 563–589.

Kolmogorov, A. N. (1941): The local structure of turbulence in incompressible viscous fluid for very large Reynolds numbers. *C. R. Acad. Sci. URSS* **30**, 301–305.

Mann, J. (1994): The spatial structure of neutral atmospheric surface layer turbulence. *J. Fluid Mech.* **273**, 141–168.

Monin, A. S. (1962): Characteristics of the scattering of sound in a turbulent atmosphere. *Sov. Phys. Acoustics* **7**, 370–373.

Ostashev, V. E. (1997): *Acoustics in Moving Inhomogeneous Media.* E & FN SPON, London.

Ostashev, V. E., B. Brähler, V. Mellert, and G. H. Goedecke (1998): Coherence functions of plane and spherical waves in a turbulent medium with the von Karman spectrum of medium inhomogeneities. *J. Acoust. Soc. Am.* **104**, 727–737.

Ostashev, V. E., and G. H. Goedecke (1998): Interference of direct and ground reflected waves in a turbulent atmosphere. In *Proceedings of the Eighth International Symposium on Long Range Sound Propagation*, Pennsylvania State University, State College, PA, 313–325.

Ostashev, V. E., and D. K. Wilson (2000): Relative contributions from temperature and wind velocity fluctuations to the statistical moments of a sound field in a turbulent atmosphere. *Acustica/Acta Acustica* (to appear).

Peltier, L. J., J. C. Wyngaard, S. Khanna, and J. G. Brasseur (1996): Spectra in the unstable surface layer. *J. Atmos. Sci.* **53**, 49–61.

Stull, R. B. (1988): *An Introduction to Boundary-Layer Meteorology*. Kluwer, Dordrecht, Germany.

Tatarskii, V. I. (1971): *The Effects of the Turbulent Atmosphere on Wave Propagation*. Keter, Jerusalem.

Wilson, D. K., and D. W. Thomson (1994): Acoustic propagation through anisotropic, surface-layer turbulence. *J. Acoust. Soc. Am.* **96**, 1080–1095.

Wilson, D. K. (1998): Performance bounds for acoustic direction-of-arrival arrays operating in atmospheric turbulence. *J. Acoust. Soc. Am.* **103**, 1306–1319.

Wilson, D. K. (2000): A turbulence spectral model for sound propagation in the atmosphere that incorporates shear and buoyancy forcings. *J. Acoust. Soc. Am.* (in review).

Wyngaard, J. C., Y. Izumi, and S. A. Collins (1971): Behavior of the refractive-index-structure parameter near the ground. *J. Opt. Soc. Am.* **61**, 1646–1650.